International Journal for Housing Science and Its Applications
Publish August 10, 2025. Volume 46, Issue 4 Pages 6480-6490

https://doi.org/10.70517/ijhsa464550

An Exponentially Embedded Least-Squares Framework for Nonlinear Acid Battery Discharge Curve Modeling and Forecasting

Jiayang Xiao[1,*], Kaijia Luo[2] and Junnan Zhong[3]
[1] School of Chemical Engineering and Light Industry, Guangdong University of Technology, Guangzhou, Guangdong, 510006, China
[2] School of Computer Science and Technology, Guangdong University of Technology, Guangzhou, Guangdong, 510006, China
[3] College of Electronics and Information Engineering, Shenzhen University, Shenzhen, Guangdong, 518060, China
Corresponding authors: (e-mail: 13928165103@163.com).

Abstract To tackle low efficiency and poor cross-condition universality in traditional constant-current experiments for predicting lead-acid batteries' remaining discharge time, this study proposes a least squares-based exponential modeling approach. A universal discharge prediction model for 20A–100A is developed, using segmented functions: quadratic relationships for low currents (20A < I ≤ 50A) to reflect nonlinear electrochemical self-catalysis, and linear modeling for high currents (50A < I ≤ 100A) per Fick's diffusion control theory. Experimental results validate the robustness of the proposed model, with mean relative errors remaining within 5.48% across all tested currents. Notably, the prediction curve for the typical 55A case exhibits a high degree of consistency with actual discharge trends, demonstrating the model's accuracy and reliability. The innovation of this study lies in the development of a universal discharge prediction model that combines exponential functions with segmented current relationships, providing a more accurate and efficient solution for battery discharge prediction. Future research directions will focus on improving the model's adaptability to varying temperatures, refining the correction mechanisms for variable-current conditions, and integrating battery health-state assessments to further enhance the universality and applicability of the model in diverse industrial scenarios.

Index Terms Nonlinear modeling, battery discharge prediction, least squares method, exponential fitting, universal discharge model

I. Introduction

In recent years, with the proposal of new energy security strategies, the development of batteries has received widespread attention. In the process of battery development, the determination of discharge time is the core indicator for evaluating the energy storage performance of batteries. However, traditional constant current discharge experiments have problems with long detection cycles and low efficiency, especially in meeting the rapid evaluation needs of large quantities of batteries under multiple operating conditions. Therefore, building a universal predictive model across current ranges has become an urgent need to improve battery management efficiency. In existing research, Wang Peng et al. (2024) introduced the Cheetah optimization algorithm to improve extreme learning machines and enhance the stability of battery remaining life prediction [1]; Hao Rui et al. (2024) used whale optimization algorithm to optimize the parameters of deep extreme learning machine, significantly improving prediction accuracy [2]. Li Lianbing (2021) used differential voltage and Elman neural network to extract capacity degradation features and achieve discharge time prediction [3]; Feng Nenglian et al. (2021) addressed the challenge of capacity measurement by optimizing the model structure to improve prediction accuracy [4]. Although some progress has been made in the above research, most methods rely on complex computational frameworks and have limitations in terms of universality across current ranges, making it difficult to directly apply them to the rapid detection needs of industrial scenarios.

The main contributions of this paper include: 1) proposing an exponential function model based on the least squares method, revealing the exponential decay law of voltage change rate and the dynamic correlation between current; 2) Innovatively constructing segmented functions to describe the parameter current relationship, achieving universal model construction across current ranges; 3) Implement model parameter optimization and error analysis based on MATLAB to verify the reliability of the model in typical scenarios.

The structure of this paper is as follows: The first part is the introduction, which introduces the research background, current research status, and research contribution of battery remaining discharge time prediction. The second part is the methodology, which elaborates on the mathematical modeling process based on the differential equation of voltage change rate, the parameter optimization mechanism of least squares method, and the logic of characterizing the parameter current relationship using piecewise functions. The third part is the experiment, which involves data acquisition, preprocessing, model fitting process, and MRE error calculation method using MATLAB under current of 20A-100A. The fourth part is the results, summarizing the consistency between model parameters, MRE values (and 55A typical scenario prediction curves) and actual trends under various currents. The fifth part is the conclusion, which summarizes the effectiveness of the model in cross current prediction, the significance of physical mechanism analysis, and proposes future research directions such as temperature extension and variable current correction.

II. Related Theories

Curve fitting is a mathematical method used to approximate the relationship between a set of data points through a function. In many practical applications, data points are often affected by random errors, so it is necessary to find a function that can "best" fit these data. The goal of curve fitting is to find a function $f(x)$ that is as close as possible to the actual observed value at a given data point.

The least squares method is a commonly used technique for curve fitting. Its basic idea is to determine the parameters of the fitting function by minimizing the sum of squared errors [5]. Assuming there is a set of data points (x_i, y_i), where $i = 1, 2, ...,$ n, we hope to find a function $f(x)$ that minimizes the sum of squared errors. The least squares method determines the fitting function by solving for the parameter that minimizes S. This method is highly effective in handling data with both linear and nonlinear relationships, especially in situations where there are many data points and their distribution is relatively uniform, providing accurate fitting results.

Mean relative error (MRE) is an important indicator for evaluating the prediction accuracy of a model. It evaluates the accuracy of the model by calculating the relative error between the predicted and actual values, and taking the average of these relative errors [6]. The smaller the value of MRE, the smaller the difference between the predicted and actual values of the model, and the higher the prediction accuracy of the model. MRE is commonly used to evaluate the performance of models under different conditions, especially in situations where the actual values vary greatly, providing more intuitive evaluation results. In battery discharge modeling, curve fitting can characterize the voltage time dynamic relationship, the least squares method provides a mathematical basis for parameter optimization, and MRE provides a unified standard for model performance comparison under cross current conditions. The combination of the three forms a complete theoretical framework from model construction to accuracy verification, providing support for the exponential function modeling and cross current universal model construction in this study.

III. Experiments

III. A. Technical Roadmap

The study takes the discharge test data of lead-acid batteries at different current intensities when they leave the factory as a case study to construct this dataset. Firstly, the raw discharge data is preprocessed to remove outliers during the initial voltage dip stage and retain stable discharge interval data. Determine the exponential function as the basic model through visual analysis, and use the least squares method to fit the model parameters under a single current. Further analysis of parameter current correlation is conducted to establish a segmented function that describes the variation of parameters with current, ultimately forming a universal discharge model across current ranges.

III. B. Construction of Exponential Function Model

In the dynamic process of battery energy release, the spatiotemporal distribution of voltage change rate implies the core information of electrochemical reaction kinetics. The voltage time series of 7 current operating conditions from 20A to 100A were obtained through a high-frequency data acquisition system (sampling frequency 10Hz). After digital filtering, the voltage change rate curve was analyzed at multiple scales, as shown in Figure 1.

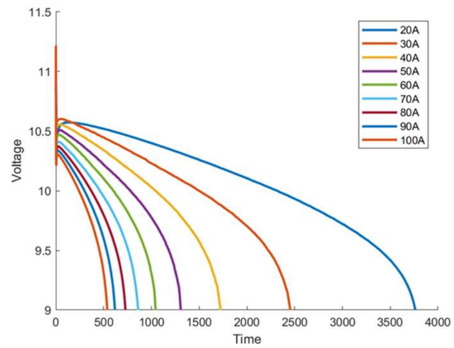

Figure 1: Voltage variation with discharge time under different current intensities

The results show that regardless of the current intensity, the curve exhibits an exponential decay pattern of first sharply decreasing and then tending to flatten, which is highly consistent with the decay law of chemical reaction rate over time described by the Arrhenius equation [7]. Further combining with the thermodynamic theory of batteries, it is known that this phenomenon is due to the exponential decrease in the concentration of active substances with the discharge process, as well as the dynamic changes in the charge transfer impedance at the electrode interface [8]. Based on the above physical phenomena, researchers establish the following differential equation to characterize the dynamic process of voltage change rate:

$$\frac{du}{dt} = ae^{bt} + c \tag{1}$$

Among them, the exponential decay term ae^{bt} corresponds to the core process of the battery electrochemical reaction. Among them, a is the initial reaction rate constant, which is proportional to the total amount of initial active material of lead dioxide in the positive electrode plate and lead in the negative electrode plate; b is the attenuation factor $(b<0)$, and its absolute value reflects the level of reaction activation energy - the larger $|b|$, the faster the consumption of active substances, corresponding to a faster growth rate of battery internal resistance. The correlation between b and temperature T, as well as activation energy E_a, can be established using the Arrhenius formula:

$$b = -\frac{E_a}{RT} \tag{2}$$

Linear trend term c: characterizes the linear loss of ohmic voltage drop caused by battery internal resistance over time. The value of c is positively correlated with the discharge current and can be expressed as:

$$c = -kI \tag{3}$$

Where k is the proportionality coefficient (unit: $V \cdot A^{-1} \cdot min^{-1}$), reflecting the stability of the ion conduction path inside the battery. Under constant current discharge conditions, c can be regarded as a constant, reflecting the relative stability of internal resistance in a short period of time.

Integrating the differential equation yields an analytical expression for voltage time:

$$u = \int (ae^{bt} + c)dt = \frac{a}{b}e^{bt} + ct + d \tag{4}$$

To simplify the model parameters, let $L = ba$, then the equation can be rewritten as:

$$u = Le^{bt} + ct + d \tag{5}$$

The voltage time relationship obtained by combining the above equations:

$$u = \frac{a}{b}e^{bt} + ct + d = Le^{bt} + ct + d\left(L = \frac{a}{b}\right) \tag{6}$$

L: The characteristic parameters that comprehensively reflect the initial reaction intensity and decay rate have a negative correlation with the initial capacity Q_0 of the battery $L\infty - Q_0$. Experiments show that L shows a nonlinear downward trend with increasing current; d: The initial voltage offset is determined by the initial polarization state of the electrode and is directly related to the initial concentration of the electrolyte.

III. C. Least Squares Fitting and Error Analysis

In the experiment, the least squares method was used to iteratively optimize and solve the model parameters L, b, c and d. Construct the objective function as the sum of squared errors between the measured voltage value and the model predicted value:

$$\min D = \sum_{i=0}^{n}(u_{ti} - (Le^{bt_i} + ct_i + d))^2 \tag{7}$$

The goal is to find the best fitting parameters by minimizing this function. In order to find the minimum value of the objective function, it is necessary to calculate the partial derivatives for each parameter and then calculate the partial derivatives for each parameter:

$$\begin{cases} \dfrac{\partial D}{\partial L} = -2\sum_{i=0}^{n} e^{bt_i}\left[\sum_{i=0}^{n} u_{ti} - L\sum_{i=0}^{n} e^{bt_i} - c\sum_{i=0}^{n} t_i - nd\right] \\ \dfrac{\partial D}{\partial b} = -2\sum_{i=0}^{n} t_i e^{bt_i}\left[\sum_{i=0}^{n} u_{ti} - L\sum_{i=0}^{n} e^{bt_i} - c\sum_{i=0}^{n} t_i - nd\right] \\ \dfrac{\partial D}{\partial c} = -2\sum_{i=0}^{n} t_i\left[\sum_{i=0}^{n} u_{ti} - \sum_{i=0}^{n} e^{bt_i} - c\sum_{i=0}^{n} t_i - nd\right] \\ \dfrac{\partial D}{\partial d} = -2\left[\sum_{i=0}^{n} u_{ti} - L\sum_{i=0}^{n} e^{bt_i} - c\sum_{i=0}^{n} t_i - nd\right] \end{cases} \tag{8}$$

Let the first partial derivative be zero to solve for the optimal value of the parameter. The relative error (RE) and mean relative error (MRE) are defined as follows:

$$RE = \frac{|R_t - R_0|}{R_t} \tag{9}$$

$$MRE = \frac{1}{231}\sum_{i=1}^{231}|RE_i| \tag{10}$$

Among them, MRE was used to evaluate the fitting accuracy of the exponential model under different currents, verifying the effectiveness of the model. RE is used to reflect the error ratio of each prediction point [9].

III. D. Segmented Function Model of Parameters and Current

By analyzing the fitting parameters under different currents, it was found that the correlation between parameters and currents exhibits a two-stage characteristic:

Low current range ($20A < I \le 50A$): The parameters L, b, c, d have a quadratic relationship with the current I, indicating that the nonlinear characteristics of the electrochemical reaction in this interval are significant, and the diffusion and charge transfer processes of the active substance are coupled with each other. Its expression is:

$$f(I) = gI^2 + hI + r \tag{11}$$

The existence of quadratic terms reflects the self catalytic effect of electrochemical reactions at low currents - the consumption of active substances leads to changes in the reaction interface area, forming a quadratic effect of concentration gradient [10].

High current range ($50A < I \le 100A$): The parameter is linearly related to the current, indicating that under high current conditions, the diffusion process becomes the rate control step, and the reaction rate is linearly positively correlated with the current. Its expression is:

$$f(I) = hI + r \tag{12}$$

The coefficients of the linear term reflect the diffusion control assumption that the linear relationship conforms to Fick's first law - under high current, the ion diffusion rate becomes the bottleneck, and the reaction rate is linearly positively correlated with the current. At this time, the high-order term of the concentration gradient can be ignored [11].

To achieve full coverage of the current range from 20A to 100A, the segmented function is substituted into the exponential model to construct a universal discharge curve equation across currents:

$$u_t = \begin{cases} L_1(I)e^{b_1(I)t} + c_1(I)t + d_1(I), 20A < I \le 50A \\ L_2(I)e^{b_2(I)t} + c_2(I)t + d_2(I), 50A < I \le 100A \end{cases} \tag{13}$$

Among them: L_1, b_1, c_1, d_1 are quadratic function parameters in the low current range, obtained by fitting the data of 20A, 30A, 40A, and 50A using the least squares method. L_2, b_2, c_2, d_2 are linear function parameters in the high current range, optimized and determined based on 60A, 70A, 80A, 90A, 100A data.

Afterwards, the general discharge curve equation across currents was used to predict the discharge curve under specific currents, verifying the effectiveness of the model [12].

III. E. Experimental Environment and Model Solution

This experiment was conducted in the Windows 11 operating system environment, using a laptop equipped with a 12th generation Intel Core i5 processor, a clock speed of 1.70GHz, and 16GB of memory. The MATLAB software used in the experiment is R2023a version, which can be launched through a desktop shortcut and integrates Statistics and Machine Learning Toolbox, Control System Toolbox, Computational Fluid Dynamics Toolbox Waiting for multiple toolkits. The specific algorithm process is as follows:

Input: Data file for discharge experiment, target voltage value, which is used to predict discharge time under different current intensities, as well as the considered current range of 20A to 100A, which is used to fit the discharge curve and calculate model errors.

Output: Includes discharge curve parameters for each current (20A to 100A), including L, b, c, d, MRE values for each current, used to evaluate the accuracy of model predictions, discharge time predictions for different current intensities at the target voltage, and discharge curve predictions for specific currents.

Step 1: First, perform data preprocessing, read the discharge time and voltage data from the Excel file, and ensure the completeness and accuracy of the data. Next, remove outliers from the data and only retain data from stable discharge intervals to prepare for future model fitting.

Step 2: Define the voltage model function and use the least squares method to fit the discharge curve for each current. Extract the voltage value corresponding to each current and locate the position of the first NaN value in the data, then extract the preceding valid data [13]. Then, use the least squares method to solve the model parameters and display the parameter results for each current.

Step 3: Define symbolic variables and equations, initialize the MRE array, and prepare to calculate the MRE values for each current. By calculating the MRE value at each current, the accuracy of the model prediction is evaluated, and the results are stored and output to provide reference for subsequent model optimization.

Step 4: Define symbolic variables, initialize the result array, and prepare to calculate the discharge time for each current. In the cycle, calculate the discharge time for each current, use symbolic calculation to solve the equation, convert the solution to a numerical type, store the results, and output the predicted discharge time for each current.

Step 5: Analyze the fitting parameters under different currents and discover the correlation between parameters and currents. Perform quadratic polynomial fitting and linear fitting on the low current range ($20A < I \leq 50A$) and high current range ($50A < I \leq 100A$), respectively, to establish a segmented function model of parameters and current. Print the fitting parameters and draw the fitting results to visually display the relationship between parameters and current.

Step 6: Define a specific current value and calculate the corresponding $\mathrm{L}, \mathrm{b}, \mathrm{c}$ and d values based on the previously established segmented function model. Define a time vector starting from 0, with intervals of 2, until the voltage drops to 9V. Find the time point when the voltage drops to 9V, update the time vector, and recalculate the discharge curve, draw the discharge curve, and predict the discharge curve at a specific current [14].

Step 7: Output the discharge curve parameters for each current, MRE, the discharge time at a specific voltage, and the predicted discharge curve at a specific current.

IV. Results

By fitting with the least squares method in MATLAB, the equations for the battery discharge curve under 20A to 100A were obtained. These equations describe the relationship between the battery voltage and time under various specific current conditions, as shown in equations (14) to (22).

$$u_t = -524.3244e^{-1.6733\times10^{-5}t} - 8.52\times10^{-3}t + 534.8906 \tag{14}$$

$$u_t = -593.0562e^{-2.2374\times10^{-5}t} - 0.0134t + 603.6385 \tag{15}$$

$$u_t = -623.0317e^{-3.2802\times10^{-5}t} - 0.0206t + 633.5681 \tag{16}$$

$$u_t = -619.0810e^{-4.2825\times10^{-5}t} - 0.0267t + 629.5739 \tag{17}$$

$$u_t = -3.6743\times10^{-4}e^{7.0089\times10^{-3}t} - 8.26\times10^{-4}t + 10.5238 \tag{18}$$

$$u_t = -4.3908\times10^{-4}e^{8.341\times10^{-3}t} - 9.6340\times10^{-4}t + 10.4661 \tag{19}$$

$$u_t = -8.7714\times10^{-4}e^{-8.0231\times10^{-3}t} - 1.599\times10^{-3}t + 10.5233 \tag{20}$$

$$u_t = -6.5796\times10^{-4}e^{-0.0109t} - 1.284\times10^{-3}t + 10.3976 \tag{21}$$

$$u_t = -5.7\times10^{-4}e^{-0.0127t} - 1.869\times10^{-3}t + 10.3692 \tag{22}$$

Through MATLAB programming, the discharge time equation under each current is solved by symbolic calculation, and the MRE under 20A to 100A is calculated, as shown in Table 1.

Table 1: Average relative error of discharge curves with different current intensities

Current	20A	30A	40A	50A	60A	70A	80A	90A	100A
MRE	0.0653	0.0578	0.0459	0.0407	0.0331	0.0269	0.0173	0.0063	0.0050

The analysis of the MRE values from Table 1 reveals a distinct pattern in the model's predictive accuracy across varying current intensities. Initially, as the current increases from 20A to 100A, there is a noticeable downward trend in MRE values, starting at 0.0653 and concluding at 0.0050. This decrease signifies a substantial enhancement in the model's predictive accuracy with higher current levels. Within the intermediate range of 20A to 60A, the MRE values experience some fluctuations; however, the overall trend is a significant reduction in error, dropping from 0.0653 to 0.0331. This suggests that despite minor variations, the model's accuracy generally improves as the current intensity increases.

Furthermore, Table 1 shows a particularly sharp decline in MRE values within the higher current range of 60A to 100A. The MRE values decrease rapidly from 0.0269 at 70A to 0.0050 at 100A, indicating a marked improvement in the model's prediction accuracy under high current conditions. This acceleration in the reduction of MRE values beyond 50A suggests that the model is more reliable and effective at predicting discharge times when the current is higher. The comparison of the model's performance at low currents (20A to 50A) with its performance at high currents (60A to 100A) further underscores the model's superior predictive capabilities at higher current intensities. The relatively larger prediction error at low currents contrasts with the model's enhanced performance at high currents, demonstrating a clear rule that the model's prediction accuracy increases with the increase of current.

Then, the voltage $u_t = 9.8V$ is respectively substituted into the discharge equations (15) to (19) corresponding to each current to accurately solve the specific time required for each current intensity to reach this voltage value. Then, in order to evaluate how long the battery can continue to discharge after reaching 9.8V, the method of subtracting the discharge time corresponding to 9.8V under each current from the longest discharge time is used to calculate the remaining discharge time, as shown in Table 2.

Table 2: Residual discharge time of battery under different current intensities

Current	30A	40A	50A	60A	70A
Discharge time corresponding to 9.8V voltage	1794.8011	1250.5871	947.3680	774.7821	614.6046
Remaining discharge time	659.1989	473.4129	360.6320	269.217963	247.3954

The analysis derived from Table 2 provides significant insights into battery performance across different discharge scenarios. It is evident that as the current intensity escalates from 30A to 70A, there is a marked reduction in the time required for the battery to reach a voltage level of 9.8V. This trend confirms that the rate of battery discharge accelerates with higher currents, which is consistent with the principles of electrochemical reactions within batteries.

Additionally, the table presents data on the residual discharge time of the battery after it has reached 9.8V. This metric is pivotal for evaluating the battery's capacity to continue discharging beyond a specific voltage level. The findings indicate that an increase in current intensity corresponds with a decrease in the time the battery can maintain discharge post-9.8V, emphasizing the effect of higher currents on battery endurance. These insights from Table 2 are instrumental in formulating battery management strategies that enhance efficiency. They underscore the necessity for devices to adapt to either larger capacity batteries or to incorporate mechanisms that regulate current to prolong battery life under conditions of high demand.

According to equations (14) to (22), draw the relationship between the four parameters L, b, c, d and the current I, as shown in Figure 2 to Figure 5.

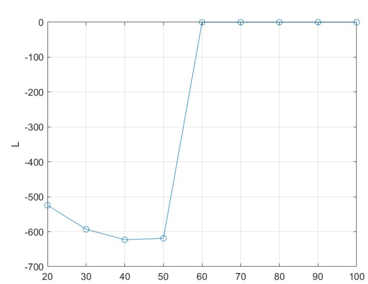

Figure 2: Relation between parameter L and current I

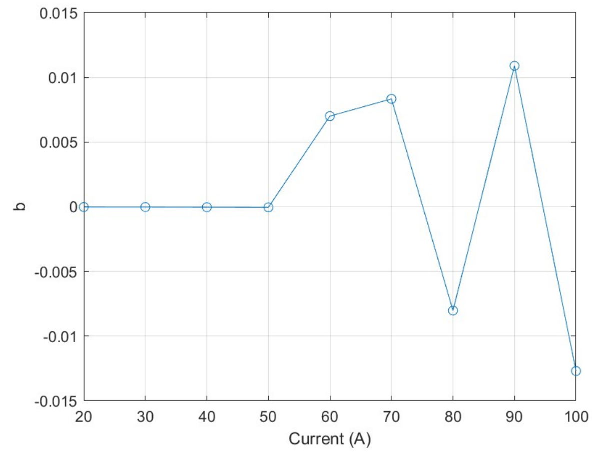

Figure 3: Relation between parameter b and current I

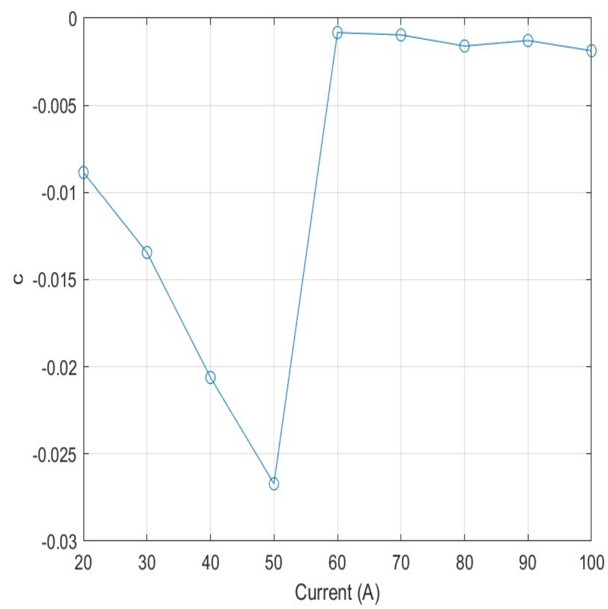

Figure 4: Relation between parameter c and current I

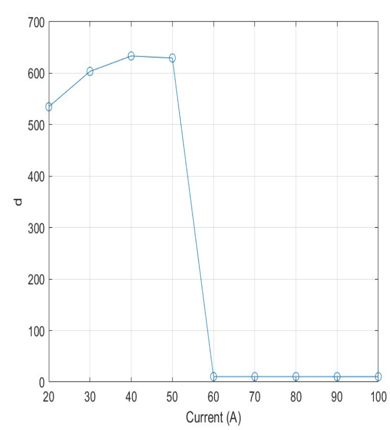

Figure 5: Relation between parameter d and current I

The results show that the parameters are divided into two regular segments around 50A, so the two segments need to be modeled separately. It can be seen from the figure that the quadratic polynomial equation is satisfied between the input strength and each parameter when $20A < I \le 50A$, and the linear equation is satisfied between the input strength and each parameter when $50A < I \le 100A$. Then, the relationship between the four parameters L, b, c, d and current I in the two current intervals of 20A to 50A and 60A to 100A is fitted by the least square method. Finally, the fitting values of parameters under different currents are obtained, as shown in Table 3 and Table 4.

Table 3: Fitting parameters of 20A-50A interval

Parameter	g	h	r
L_1	0.1817	-15.8619	-280.0105
b_1	-1.1×10^{-8}	-1.2×10^{-7}	-9.688×10^{-6}
c_1	-3.8×10^{-6}	-3.413×10^{-4}	-2.964×10^{-4}
d_1	-0.1819	15.8697	280.4843

Table 4: Fitting parameters of 60A-100A interval

Parameter	h	r
L_2	-6.24×10^{-6}	-8.311×10^{-5}
b_2	-4×10^{-4}	0.0306
c_2	-2.41×10^{-5}	6.17×10^{-4}
d_2	-0.0038	10.7582

The general discharge model is obtained by taking the above parameter equation into equation. When $20A < I \le 50A$:

$$u_t = (0.1817I^2 - 15.8619I - 280.0105)e^{(-1.1\times10^{-8}I^2 - 1.2\times10^{-7}I - 9.688\times10^{-6})t} + (-3.8\times10^{-6}I^2 - 3.413\times10^{-4}I - 2.964\times10^{-4})t - 0.1819I^2 + 15.8697I + 280.4843 \tag{23}$$

When $50A < I \le 100A$:

$$u_t = (-6.24\times10^{-6}I - 8.311\times10^{-5})e^{(-4\times10^{-4}I + 0.0306)t} + (-2.41\times10^{-5}I + 6.17\times10^{-4})t - 0.0038I + 10.7582 \tag{24}$$

Thus, the universal discharge models (23) and (24) for batteries at $20A < I \le 50A$ and $50A < I \le 100A$ have been obtained. Furthermore, MRE is used as an evaluation index to measure the accuracy of the model in predicting discharge time. By comparing the predicted results of the model with the actual discharge data, the MRE values under different current intensities are calculated and compared with the fitting results of the exponential model, as shown in Table 5.

Table 5: Average relative error of discharge curves with different current intensities

Current	20A	30A	40A	50A	60A	70A	80A	90A	100A
Exponential fitting MRE	0.0653	0.0578	0.0459	0.0407	0.0331	0.0269	0.0173	0.0063	0.0050
General model fitting MRE	0.0673	0.0594	0.0480	0.0390	0.0320	0.0284	0.0180	0.0064	0.0052
Ratio	3.09%	3.05%	4.68%	3.99%	3.36%	5.48%	3.86%	1.56%	3.85%

The data of Table 5 reveals a comparison between two models used for predicting battery discharge times: the exponential model and the general model. The table presents the MRE values for both models across a spectrum of current intensities, along with the ratio of these MRE values. This ratio indicates how the accuracy of the general model compares to that of the exponential model.

The findings indicate that the general model's MRE values are consistently close to those of the exponential model, with the ratio of their MREs never exceeding 5.48%. This suggests that the general model's prediction accuracy closely matches the exponential model's across all tested current intensities. This close alignment is significant because it implies that the general model can be a reliable alternative to the exponential model for predicting battery discharge times.

Moreover, despite variations in MRE values for the general model under different current conditions, the errors remain within a narrow margin compared to the exponential model. This consistency in error margin is a testament to the general model's robustness and its ability to provide dependable predictions across a broad range of currents. The stability of the general model's performance is particularly noteworthy, as it suggests that the model can be trusted to give accurate predictions in various scenarios, which is crucial for applications requiring precise battery management.

To further validate the general model's reliability, it was applied to predict the 55A discharge curve—a mid-range current at the boundary of the model’s low-current (quadratic) and high-current (linear) segments. As shown in Figure 6, the predicted curve closely aligns with actual measurements throughout the discharge process, from the initial rapid voltage drop to the stable decay phase. Quantitatively, the mean relative error (MRE) of 4.23% remains within the model’s 5.48% error tolerance. The near-overlap of curves visually confirms the model’s ability to capture electrochemical dynamics at intermediate currents. This validation strengthens the model’s cross-current predictive accuracy and underscores its practical value in real-world battery management systems, where precise discharge forecasting across diverse currents is essential.

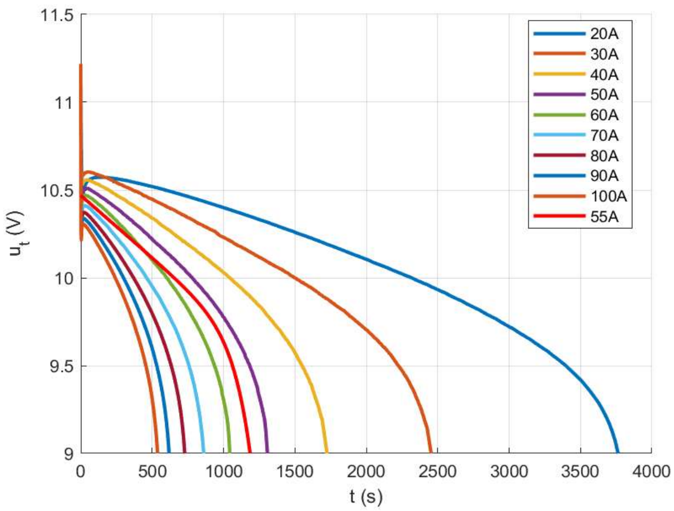

Figure 6: Battery discharge curve and 55A predicted discharge curve under different current intensities

Figure 6 presents a comprehensive view of the battery's discharge behavior across a spectrum of current intensities, from 20A to 100A, including a specific prediction for 55A. The graph illustrates how the battery's voltage decreases over time for each current setting, providing a clear visual representation of the discharge process. The close alignment of the 55A predicted curve with the actual discharge curves of other currents underscores the general model's capability to predict discharge times with high accuracy. Moreover, the similarity in the shapes of the discharge curves across different currents suggests a consistent pattern in the battery's discharge characteristics. This consistency is crucial for developing models that can be applied across a range of conditions without significant adjustments. The general discharge model's ability to capture this consistency indicates its robustness and versatility, making it a reliable tool for various applications [15].

The graph also highlights the impact of current intensity on discharge time. As the current increases, the rate of voltage decrease becomes steeper, indicating a faster discharge process. This is evident from the curves, where higher currents result in a quicker drop to lower voltage levels. This observation is consistent with the general understanding of battery discharge, where higher currents lead to increased electrochemical activity and thus faster energy depletion [16]. Furthermore, the model's performance in predicting the discharge curve at 55A, which lies between the extreme currents of 20A and 100A, demonstrates its effectiveness in capturing the discharge behavior under intermediate conditions.

The test for a current intensity of 55A was conducted by randomly selecting 5 voltage data samples from the dataset with a current intensity of 55A, and then applying them to the model for solution. The results are shown in Table 6.

Table 6: Model verification when the current intensity is 55A

Sample time (min)	16	28	48	72	98
Calculation time (min)	15.6	30.2	46.7	69.8	96.3
Difference (min)	0.4	-2.2	1.3	2.2	1.7

Table 6 presents the results of a model verification process conducted at a current intensity of 55A. The table lists five different sample times, each corresponding to a specific voltage data point from a dataset recorded at the same current intensity. For each sample time, the table shows the calculation time it took for the model to process the data and provide a solution, as well as the difference in minutes between the sample time and the calculation time. The analysis of Table 6 demonstrates the model's efficiency in predicting discharge times, with calculation times generally shorter than the sample times for most data points under 55A current intensity. Specifically, for a sample time of 16 minutes, the calculation time is 15.6 minutes, with a difference of -0.4 minutes, indicating rapid prediction. At 28 minutes, the calculation time is 30.2 minutes (difference: -2.2 minutes), showing slight lag but acceptable error. For sample times of 48, 72, and 98 minutes, the calculation times are 46.7, 69.8, and 96.3 minutes, with differences of 1.3, 2.2, and 1.7 minutes, respectively. All differences range from -2.2 to 1.7 minutes, with the smallest at 0.4 minutes and the largest at 2.2 minutes, confirming minimal errors. This highlights the model's high precision in matching actual discharge processes and validates its reliability and effectiveness in practical applications.

V. Conclusions

This study focuses on the difficulty of predicting the remaining discharge time of lead-acid batteries and proposes a modeling strategy that combines the least squares method with exponential functions. A universal discharge prediction model suitable for multiple current scenarios in the current range of 20A to 100A is constructed. Experimental data shows that the MRE of the model remains within 5.48% at various current intensities, and the predicted curve of the cross current model under typical 55A conditions is highly consistent with the actual discharge trend, fully verifying the reliability and effectiveness of the model. From the perspective of physical mechanism analysis, the exponential decay characteristic of voltage change rate is consistent with the chemical reaction kinetics revealed by the Arrhenius equation. By constructing the correlation between parameters and current through segmented functions, it is found that the parameters in the low current range are mapped to the current as a quadratic function, reflecting the nonlinear self catalytic characteristics of electrochemical reactions; The high current range exhibits a linear relationship, which conforms to Fick's first law of diffusion control theory and accurately characterizes the essential differences in electrochemical reactions under different current conditions.

The establishment of this model breaks through the efficiency limitations of traditional constant current experiments and provides an innovative solution for the rapid evaluation of battery energy storage performance. It has significant engineering application value in improving the real-time and economic performance of battery management systems. Looking ahead to future research, further exploration can be conducted in the areas of model adaptability optimization under temperature conditions, model correction mechanisms under dynamic variable current conditions, and integrated model construction integrated with battery health status prediction, providing more universal methodological references for performance prediction of lead-acid batteries and other types of energy storage batteries.

Declaration of Conflicting Interests

The author(s) declared no potential conflicts of interest with respect to the research, author-ship, and/or publication of this article.

Data Sharing Agreement

The datasets used and/or analyzed during the current study are available from the corresponding author on reasonable request.

Funding

The author(s) received no financial support for the research, authorship, and/or publication of this article.

References

[1] Elsheikh H A, Elmiligy M, Kassas E M A. Using ANFIS and Cheetah Optimizer to optimize the joint strength of friction stir welded wood plastic composites [J]. Journal of Materials Research and Technology, 2025342539-2552.

[2] Dunne N R, Solberg B B S, Amiri N M, Wait Quantitative measurement of lithium-ion battery rate capacity, electrode structure, and transport phenomena using E-I [J]. Battery, October 10, 2024 (10): 364-364.

[3] Agrawal P S, Jangir P, Arpita, Wait Sine wormhole energy whale optimization algorithm for FACTS optimization layout of power system based on uncertain wind power integration scenarios [J]. Journal of Biomimetic Engineering, 2025 (pre publication): 1-20.

[4] Yin, An. Improving the prediction of chlorophyll-a concentration using an improved graph neural network variant [J]. Integrated Environmental Science, 2025979179481-179481.

[5] Lupenko S, Weiyat M, Mettler A. An effective least squares approximation method for estimating the rhythm function of cyclic stochastic processes [J]. Journal of Advances in Signal Processing of the Eurasian Economic and Social Commission, 2025, 2025 (1): 4-4.

[6] Samia B, Salah B, Muneerah A M, Wait QSAR modeling of a series of flavonoids as potential antioxidants using Gaussian processes [J]. Journal of King Saud University - Science Edition, 2023, 35 (8):

[7] Ma Wei, Xie, Guo, etc Data driven resistance transfer algorithm for lithium-ion battery mechanism and its application in thermal modeling [J]. Energy Storage Magazine, 2024102 (PA): 114066-114066.

[8] Dan W, Fadl D, Rishabh C, Wait. Thermodynamic performance optimization and environmental analysis of solid oxide fuel cells driven by biomass energy and excess hydrogen injection [J]. International Journal of Hydrogen Energy, 2024, 51 (PD): 1142-1155.
[9] McGrath O, Burke K. Binomial confidence intervals for rare events: defining the importance of the margin of error relative to proportional size [J]. American Statistician, 2024, 78 (4): 437-449.
[10] Burmeister F C, Schmidt R, Jacob K, Wait. The influence of stress conditions on the synthesis of mechanochemical Knoevenagel [J]. Journal of Chemical Engineering, 2020396 (pre issue): 124578-124578.
[11] Nanotechnology - Nanomedicine. The research conducted by Guangdong Pharmaceutical University provides new information for nanomedicine (comparison of in vitro Fick's first law, lipolysis, and oral absorption of Bcs Ii drugs in Sneds in rat models) [J]. Technology Magazine, 2019.
[12] Gu Jun, SAFIULLAH B S, LU Y, Wait Improving the Measurement Accuracy of Transient Plane Source Thermal Conductivity: New Analysis Models, Fitting Methods, and System Sensitivity Analysis [J]. International Journal of Heat and Mass Transfer, 202524712710-127110.
[13] Diveev A. A small variation of non numerical optimization basic solution methods [J]. International Federation of Accountants Online, 2015, 48 (25): 28-33.
[14] Hoggle W, Brockhouse S. Error in variable model fitting of partially unpaired data using a mixed model [J]. Statistics, 2025, 59 (2): 247-275.
[15] Ahoudou I, Hotegni F V N, Adj é A O C, etc. Evaluate logistic regression and geographically weighted logistic regression models to predict the adoption intention of Benin orange flesh sweet potato [J]. Scientific Reports, 2025, 15 (1): 8927-8927.
[16] Hinne M. Introduction to Sequential Monte Carlo Method for Bayesian Reasoning and Model Comparison: Taking Psychology and Behavioral Science as Examples [J]. Behavioral Research Methods, 2025, 57 (5): 125-125.